Topological patterns in two-dimensional gel electrophoresis of DNA knots

Davide Michieletto[a,1], Davide Marenduzzo[b], and Enzo Orlandini[c]

[a]Department of Physics and Complexity Science, University of Warwick, Coventry CV4 7AL, United Kingdom; [b]School of Physics and Astronomy, University of Edinburgh, Edinburgh EH9 3FD, United Kingdom; and [c]Dipartimento di Fisica e Astronomia and Sezione, Istituto Nazionale di Fisica Nucleare, Universitá di Padova, 35131 Padova, Italy

Edited by Tom C. Lubensky, University of Pennsylvania, Philadelphia, PA, and approved August 14, 2015 (received for review April 9, 2015)

Gel electrophoresis is a powerful experimental method to probe the topology of DNA and other biopolymers. Although there is a large body of experimental work that allows us to accurately separate different topoisomers of a molecule, a full theoretical understanding of these experiments has not yet been achieved. Here we show that the mobility of DNA knots depends crucially and subtly on the physical properties of the gel and, in particular, on the presence of dangling ends. The topological interactions between these and DNA molecules can be described in terms of an "entanglement number" and yield a nonmonotonic mobility at moderate fields. Consequently, in 2D electrophoresis, gel bands display a characteristic arc pattern; this turns into a straight line when the density of dangling ends vanishes. We also provide a novel framework to accurately predict the shape of such arcs as a function of molecule length and topological complexity, which may be used to inform future experiments.

DNA knots | topology | gel electrophoresis

Topology plays a key role in the biophysics of DNA and is intimately related to its functioning. For instance, transcription of a gene redistributes twist locally to create what is known as supercoiling, whereas catenanes or knots can prevent cell division; hence they need to be quickly and accurately removed by specialized enzymes known as topoisomerases. How can one establish experimentally the topological state of a given DNA molecule? By far the most successful and widely used technique to do so is gel electrophoresis (1, 2). This method exploits the empirical observation that the mobility of a charged DNA molecule under an electric field depends on its size, shape, and topology (2). Gel electrophoresis is so reliable that it can be used, for instance, to map replication origins and stalled replication forks (3), to separate plasmids with different amount of supercoiling (3, 4), and to identify DNA knots (5, 6). The most widely used variant of this technique nowadays is 2D gel electrophoresis, where a DNA molecule is subjected to a sequence of two fields, applied along orthogonal directions (2). The two runs are characterized by different field strengths and sometimes also gel concentrations (4); with suitable choices, the joint responses lead to increased sensitivity.

Although gel electrophoresis is used very often, and is extremely well characterized empirically, there is still no comprehensive theory to quantitatively understand, or predict, what results will be observed in a particular experiment. Some aspects are reasonably well established. For instance, it is now widely accepted that the physics of the size-dependent migration of linear polymers can be explained by the theory of biased polymer reptation (7–12). Likewise, the behavior of, for example, nicked, torsionally relaxed, DNA knots in a sparse gel and under a weak field is analogous to that of molecules sedimenting under gravity (13–15). The terminal velocity can be estimated via a balance between the applied force and the frictional opposing force, which is proportional to the average size of the molecule; as a result, more-complex knots, which are smaller, move faster under the field. However, the mechanisms regulating the electrophoretic mobility of DNA knots at intermediate fields, and in more-concentrated agar gels, are much less understood (4, 13, 16). Here, experiments suggest that the mobility of knots is usually a nonmonotonic function of the knot complexity, or, more precisely, of their average crossing number (5, 17) (ACN): Initially, knots move more slowly as their ACN increases, whereas, past a critical ACN, more-complex knots move faster. The combination of the responses to external fields directed along two perpendicular directions leads to a characteristic electrophoretic arc, which allows separation of the first simple knots more clearly in a 2D slab (4, 6, 18, 19). To our knowledge, there is currently no theoretical framework that quantitatively explains the nonmonotonic behavior at intermediate or large fields and the consequent formation of arc patterns.

To address this issue, here we present large-scale Brownian dynamics simulations of knotted DNA chains migrating through a gel, and subjected to a sequence of fields of different strength and direction, as in 2D gel electrophoresis experiments (see cartoon in Fig. 1*A*). We model the gel as an imperfect cubic mesh (20), where some of the bonds have been cut (see *Materials and Methods*) to simulate the presence of open strands, or dangling ends, which have been observed in physical agarose gels (21–27). Our results confirm the linear relation of the electrophoretic mobility with ACN for the first simple knots (we study ACN up to 12) in a sparse gel and under a weak field. However, our simulations also suggest that, due to a nonnegligible probability of forming "impalements" where a dangling end of the gel pierces a knot, the response of the chain to stronger fields is different. We suggest that, in this regime, the sole radius of gyration is not enough to explain the observed dynamics, and we introduce an average "entanglement number" that increases with the ACN and provides a measure of the likelihood of forming an

Significance

Gel electrophoresis is a ubiquitous biophysical technique. It consists of dragging charged biopolymers through a porous gel, by applying an electric field. Because the migration speed depends on topology, this method can be used to classify DNA knots. Currently, electrophoresis relies on empirical observations, and its theoretical understanding is limited. No theory can explain why knot mobility under strong fields depends nonmonotonically on complexity. Our study reveals a possible reason: Although complex knots have a smaller size, and hence move faster through the gel, they can become severely entangled with the gel, causing longer pauses. Our results can improve the design of future electrophoresis experiments.

Author contributions: D. Michieletto, D. Marenduzzo, and E.O. designed research; D. Michieletto performed research; D. Michieletto analyzed data; and D. Michieletto, D. Marenduzzo, and E.O. wrote the paper.

The authors declare no conflict of interest.

This article is a PNAS Direct Submission.

[1]To whom correspondence should be addressed. Email: d.michieletto@warwick.ac.uk.

This article contains supporting information online at www.pnas.org/lookup/suppl/doi:10.1073/pnas.1506907112/-/DCSupplemental.

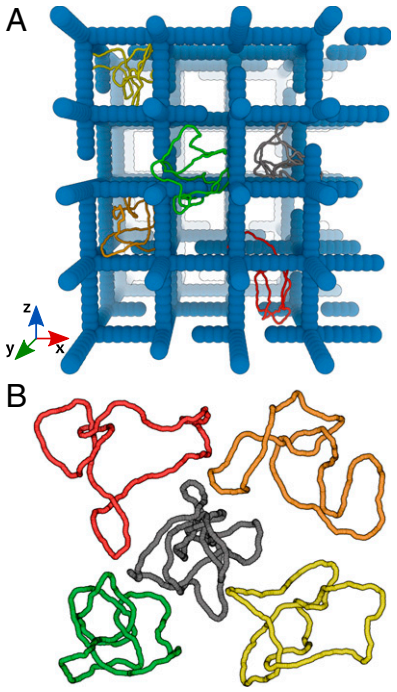

Fig. 1. (*A*) Snapshot (to scale) of the model gel with some examples of knotted configurations. Note that, to model a physical gel, a simple cubic structure is randomly cut to create dangling ends. (*B*) Equilibrium configurations of some of the knots considered; it can be readily seen that the size tends to be smaller as the knot becomes more complex. The knots pictured in *A* and *B* are trefoil (3_1), red; figure of eight (4_1), orange; pentafoil (5_1), yellow; Stevedore's (6_1), green; and nonafoil (9_1), gray.

impalement. The time needed by a knot to disentangle from the gel increases with its average entanglement number (AEN), or knot complexity, and this slows down the motion, thus competing with the Stokes friction, which leads to an increase of mobility with ACN. As a result of this contest, one typically gets a nonmonotonic behavior of the terminal speed with ACN, and an electrophoretic arc in two dimensions.

We also provide a simple model, based on a mapping between the DNA knot dynamics and a biased continuous-time random walk, which faithfully reproduces our Brownian dynamics simulations starting from a minimal number of assumptions. This approach can then be used to predict how the shape of the electrophoretic arc should depend on system parameters such as the average lattice spacing (pore size) of the gel and the contour length of DNA knots; as we shall see, the predicted trends are in agreement with existing 2D electrophoresis data. This constitutes, to our knowledge, the first example of a quantitative prediction of 2D electrophoretic diagrams; hence we suggest that the approach we present could potentially lead to even more accurate and targeted experiments to separate topoisomers in DNA or other polymers.

DNA Knots Form an Electrophoretic Arc only in Irregular Gels

The system we studied, sketched in Fig. 1 (see also *Materials and Methods* and *Supporting Information*), consists of 10 nicked, i.e., torsionally relaxed, DNA loops of ∼3.7 kilobase pairs (kbp) within a model agarose gel with dangling ends. These loops are either unknotted or form one of the first few simple knots [with up to nine crossing in their minimal projection (28)]. The loops were first equilibrated within the gel (see *Supporting Information*) and then subjected to an in silico gel electrophoresis process where a weak electric field is first applied ($\lesssim 50$ V/cm) along the vertical (z) direction, followed by a stronger field ($\gtrsim 150$ V/cm) along a transversal, say y, direction. We refer to these two fields as "weak" and "stronger," or "moderate," in what follows. The complete equations of motions and force fields used in our Brownian dynamics simulations are detailed in *Supporting Information*.

By monitoring the trajectories of the knots through the gel, we computed the average speed of their center of mass along each of the field directions (see *Supporting Information* and Fig. 2 *A* and *B*). As expected, the mobility along the direction of the weak field increases with the topological complexity of the configurations. Along the direction of the moderate field, however, the mobility of the knots displays a nonmonotonic behavior. In particular, the unknot now moves faster than either the trefoil or the 4_1 twist knot, and has an average speed similar to the 5_1 knot. This nonmonotonic behavior of the knot mobility, as a function of the ACN, was previously observed in typical experiments with torsionally relaxed DNA knots (4, 6, 18, 19, 29). It is worth noticing that, within the five-crossings family, the 5_1 torus knot moves more slowly than the 5_2 twist knots. This is similar to what was observed in the weak field case (although much less enhanced) but different from what is observed in experiments of sedimentation (15).

To better compare our findings with experiments, we report, in Fig. 2*C*, the spatial distribution of the knots as Gaussians centered in $[v_z(\mathcal{K})t_z, v_y(\mathcal{K})t_y]$ where $v_z(\mathcal{K})$ and $v_y(\mathcal{K})$ are the velocities along z (weak field direction) and y (stronger field direction) of knot K, and t_y and t_z are the electrophoretic run times. The width of the Gaussians is set to be proportional to the SD of the velocities. The resulting spots can be seen as the in silico analog of the ones observed in gel electrophoretic experiments. Note that the combination of a monotonic behavior along the weak field direction with a nonmonotonic one along the stronger field gives rise to the arc-shaped distribution of the spots characteristic of 2D electrophoresis experiments run either on knotted configurations or on supercoiled plasmids (4) (see Fig. 2*D*).

It is interesting to ask whether one can observe the electrophoretic arc also in simulations where the gel is a regular cubic mesh, i.e., a mesh with no dangling ends, as this has been, so far, the typical way to model an agarose gel (16). Remarkably, unlike the case of gel with dangling ends, also called "irregular" hereafter, no example of nonmonotonic behavior of the knot mobility is found for regular gels (for comparison, see Fig. 2*C* and Fig. S1). This result is in line with previous simulations based on lattice knots in regular gels (16) and persists for different field strengths (1.25 – 600 V/cm) and gel pore sizes (200 – 500 nm) (see *Supporting Information*). [We note that physical gels also have an inhomogeneous pore size; although considering this aspect will affect our results quantitatively, the common understanding is that the knot speed should depend monotonically on size (1). This is qualitatively different from the case of dangling ends, where the gel–polymer interactions strongly depend on topological complexity as well.] Hence our simulations strongly suggest that the causes for the nonmonotonic behavior, observed in the case of irregular gels, are to be sought in the interaction between the knots and the gel dangling ends.

This conjecture is also supported by the fact that linear (open) DNA samples are frequently observed to migrate faster than covalently closed (unknotted) ones in gel electrophoresis experiments performed in both strong and weak fields (4, 6, 18, 29). This is in line with the outcome of a recent computer experiment probing the dynamics of linear and unknotted circular molecules through an irregular gel (20).

DNA Samples Become Severely Entangled with the Dangling Ends

Having established that the presence of dangling ends in gels severely affect the transport properties of the knotted DNA loops under moderate electric fields, it is natural to look at the possible mechanisms ruling this phenomenon.

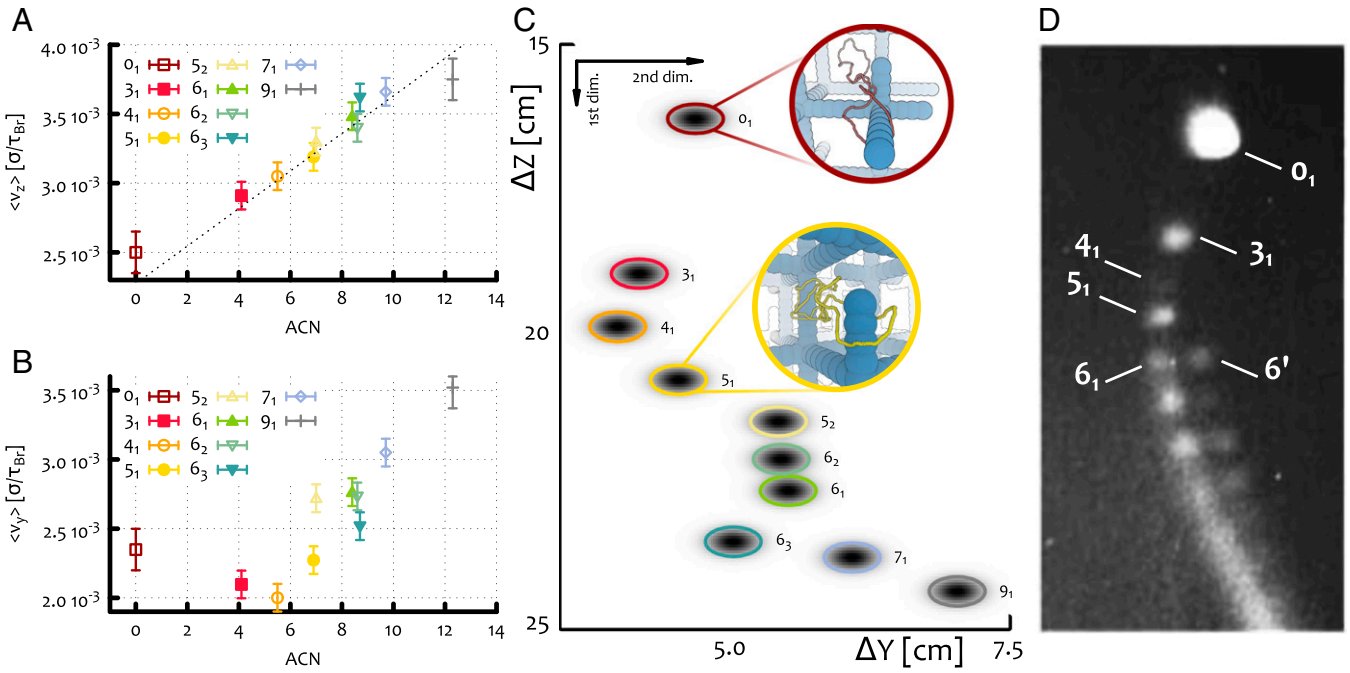

Fig. 2. In silico 2D gel electrophoresis for knotted DNA loops. (*A*) Average velocity of different types of knotted polymers along the direction of the weak electric field: $E_1 = f_1/q_b \simeq 50$ V/cm. The dotted line indicates the linear increase with the ACN. (*B*) Average velocity of different types of knotted polymers along the direction of the moderate field $E_2 = f_2/q_b = 150$ V/cm. (*C*) A 2D reconstruction of the spatial distribution of the knots as Gaussian probability distributions centered in $[v_z(\mathcal{K})t_z, v_y(\mathcal{K})t_y]$, where $v_z(\mathcal{K})$ and $v_y(\mathcal{K})$ are the average speeds along, respectively, the weak and stronger field direction of knot type K, as found by Brownian dynamics simulations. The electrophoretic run times correspond to $t_z = 0.8\ 10^{10}\ \tau_{Br} \simeq 5$ min and $t_y = 2.6\ 10^{10}\ \tau_{Br} \simeq 16$ min. The spread of each spot has been estimated by looking at the SD of $v_z(\mathcal{K})$ and $v_y(\mathcal{K})$. (Examples of single trajectories along the z and y directions are reported in Fig. S1). (*D*) Outcome of a 2D gel electrophoresis experiment performed on P4 viral DNA (10 kbp) at 0.4% agarose concentration [reprinted with permission from ref. 6 (Arsuaga et al.)].

The typical trajectories and average extension of some knotted loops as they move through a regular model gel and a gel with dangling ends are markedly different at moderate fields (see Fig. S1). In a regular gel, knots respond to the field, by shrinking their size so as to channel through the pores of the gel more efficiently. This mechanism, also known as "channeling," in which polymers squeeze through the gel pores, has already been observed in previous works (30, 31), and it was previously conjectured to play a role in the nonmonotonic separation of DNA knots in gels, as more-complex knots could have a different ability in deforming their overall shape when squeezing through the pores (4). On the other hand, as discussed in *DNA Knots Form an Electrophoretic Arc*, we find that this behavior is not sufficient to explain the electrophoretic arc, as, for regular gels, we always observe a monotonic separation of the knots as a function of the ACN (see Fig. S1). Conversely, in the case of irregular gels, knotted loops are much more prone to entangle with one (or more) dangling ends (see *Insets* of Fig. 2*C* for some examples). These entangled states (or impalements) require some time to be unraveled, and this is the reason for the anomalously long pauses observed in the knot trajectories (see, in particular, Fig. S1). Clearly, as the DNA gets longer, impalements, which can either be parallel or perpendicular with respect the direction of the field, become progressively more likely. As a matter of fact, this could be one of the reasons why it is, in practice, unfeasible to perform efficient gel electrophoresis experiments with circular DNA longer than 10 kbp (32): At these sizes, impalements are so frequent that they may cause DNA breakage.

In analogy with the phenomenon of threading, which slows down the dynamics of unknotted loops either in a melt or in a gel (20, 33, 34), and that of "crawling" of knots around obstacles (35), it is reasonable to expect that more-complicated knots will take longer to disentangle themselves from an impalement. We argue that this mechanism, when competing with the reduced Stokes drag of more-complex knots in gels, is ultimately responsible for producing a nonmonotonic dependence as a function of their complexity, i.e., their ACN.

More-Complex Knots Have Smaller Size but Larger Entanglement Number

Given that impalement events are key factors in determining the mobility of DNA knots within gels with dangling ends, it is important to find a way to define and measure this entanglement. Impalement may occur with dangling ends oriented along several directions (see examples in Fig. 2*C*), but it is reasonable to expect that all these events involve a similar mechanism in which, i.e., one dangling end "pierces through" the knot.

To quantify the degree of knot–gel entanglement, we consider an equilibrated knot configuration in the gel, and project it on the plane perpendicular to the field direction. We then choose randomly a base point P, at a distance from the projection plane that is much bigger than the radius of gyration of the projected configuration, R_g^{proj}. Starting from P, we draw an arc that pierces only once the projection plane at a point, Q, chosen randomly, with uniform probability within a disk of radius R_g^{proj} and centered in the center of mass of the projected configuration. The arc and the plane define a semispace, and we close the path with a second arc connecting Q and P and living in the other semispace (see Fig. 3*A*). To assess whether this circular path interacts topologically with the knotted configuration, we compute the absolute value of the linking number, $|Lk|$, between the circular path and the knot. Fig. 3 *B* and *C* shows the result of this procedure when applied to two different knotted loops. By averaging $|Lk|$ over several circular paths with different Q, and over different knot configurations, we define the AEN, $\langle\pi\rangle$, as the measure of the degree of entanglement between the knotted loops and the surrounding gel.

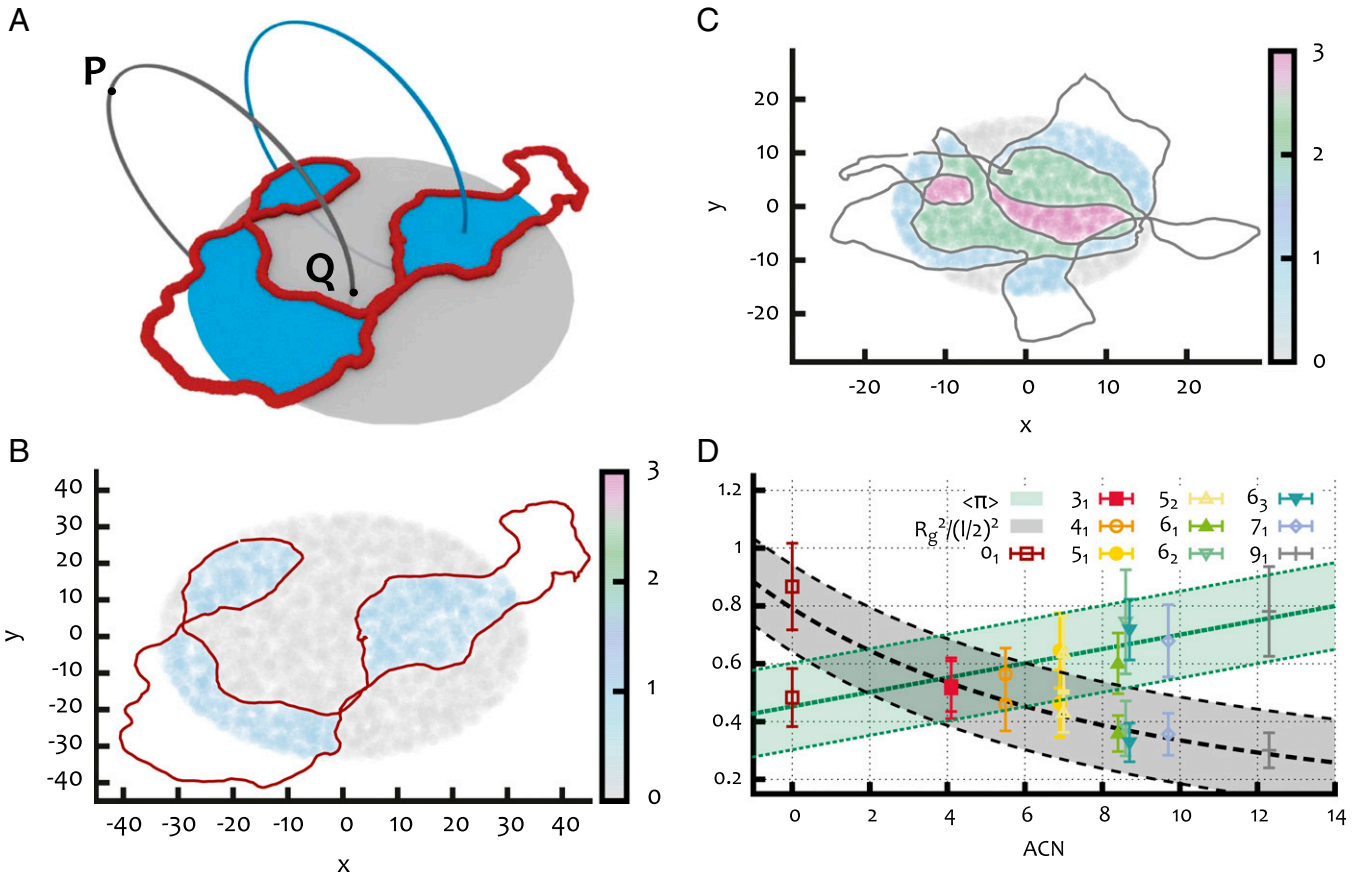

Fig. 3. (*A*) Sketch of the procedure used to define the piercing, or entanglement number: For a given projection of the configuration, the crossings define a set of regions whose intersections with the disk of radius R_g^{proj} are highlighted in blue. Starting from different points *P* far away from the projections, closed paths (two in the example) that pierce the disk once at different locations *Q* are built at random. The absolute value of the linking number is then computed between the knot configuration and each closed path. The average over the set of closed paths is finally taken: This is the AEN. *B* and *C* show the results of the procedure described in *A* for a configuration with knot type 9_1 (*C*) and for an unknotted configuration (*B*). The regions are colored according to the computed absolute value of the linking number (see color map at left). Note that for the 9_1 case, there are regions of high $|Lk|(3)$, which are more prone to become entangled with the dangling ends of the gel. (*D*) The AEN $\langle\pi\rangle$ and the mean squared radius of gyration divided by $(l/2)^2$ (*l* is the gel pore size) for different knot types classified in terms of ACN.

From Fig. 3*D*, we see that $\langle\pi\rangle$ grows approximately linearly with can; as one would expect, more-complex knots can, on average, become more entangled with the surrounding irregular gel. It is interesting to compare this behavior with that of the mean squared radius of gyration normalized with respect to half the gel pore size (see Fig. 3*D*): Unlike the AEN, the average extension of the loop is, to a good approximation, inversely proportional to the ACN, i.e., to the knot complexity. This corresponds to the well-known fact that, for a given loop contour length, more-complex knots are on average less extended (5, 15) (see also the equilibrium configurations in Fig. 1).

The plots in Fig. 3*D* suggest a possible interpretation of the nonmonotonic mobility of the knots in irregular gels based on the interplay between the average size and the degree of entanglement with the gel. On one hand, more-complex knots, being smaller in size, experience less frequent collision with the gel and hence should travel more easily through it; this is just another variant of the Stokes friction argument discussed previously. On the other hand, once knot–gel collisions occur, more-complex knots experience a more intricate entanglement with the gel (higher values of AEN are more probable) that will take longer to unravel (5, 14, 16, 35).

The above argument suggests the existence of two time scales in the process: one is the time τ_f between two successive knot–gel collisions yielding a local entanglement; the other, $\tau_{\rm dis}$, is the time needed by the knotted loop to fully disentangle from the impalement. The time scale τ_f increases as the knot average size decreases, and hence increases with knot complexity (ACN). In other words, more-complex knots experience, on average, less collisions with the gel than their simpler counterpart. The second time scale, $\tau_{\rm dis}$, is instead an increasing function of $\langle\pi\rangle$ (see Fig. 3*D*) and hence of the knot complexity (measured in terms of ACN). According to this picture, the slowest topoisomer in an irregular gel with a given lattice spacing will be the one with the best compromise between a high rate of collisions, and a sufficiently high value $\langle\pi\rangle$.

To investigate more quantitatively the dependence of τ_f and $\tau_{\rm dis}$ on the knot type (ACN), we analyze the trajectories of the knotted loops in the gel by computing (*i*) the average number of times a knot arrests its motion in the gel (entanglement event), $\langle n_e\rangle$, and (*ii*) the distribution of the duration of these entanglement events.

As specified in *Supporting Information*, the duration of the entanglement events can be identified as the time intervals where the spatial position of the center of mass of the configuration deviates significantly from the expected collision-free field-driven linear motion with speed $v_{free} = F_{z,y}/M\zeta = f_{z,y}/\zeta$.

As reported in *Supporting Information* (Fig. S2), the average fraction of time in which the knot is trapped, τ_w/τ_{tot} (τ_{tot} is the time of the full trajectory), is a nonmonotonic function of the ACN, in line with the result on the mobility under moderate field (Fig. 2*B*). In Fig. 3*A*, we show that the average number of entanglement

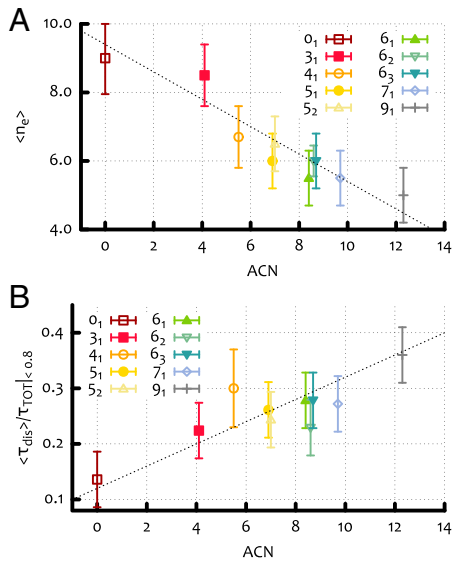

Fig. 4. (*A*) Average number of events in which the knot is entangled with the surrounding gel (entanglement events) as a function of ACN. (*B*) Average disentanglement time as a function of ACN. In these estimates, only entanglement events with duration shorter than 200 τ_{Br} are considered.

events $\langle n_e \rangle$ decreases with the knot complexity (i.e., ACN). On the other hand, the distribution of the duration of these events displays an intriguing bimodal shape, with two peaks occurring respectively at short and very long times (see Fig. S3). The peak at long times can be interpreted as the signature of head-on collisions with the gel, where the dangling ends involved are opposite to the direction of the knot motion. The resulting entanglement is, in this case, very difficult to unravel, especially in the presence of a strong electric field (see, for instance, *Inset* of Fig. 2 for the unknot). Nonetheless, whether or not we exclude from the statistic the entanglement events corresponding to the peak at long times, the characteristic disentanglement time $\tau_{\rm dis}$ turns out to increase (linearly) with the knot complexity, i.e., with ACN (see Fig. 4*B*).

We assume that this bimodal shape is due to a shift in the energy barrier that the knots have to overcome to disentangle from the dangling ends. In particular, one can think of this process as an Arrhenius process, where the energy barrier is a function of the length (projected along the field direction) of the dangling end, the knot complexity, and, more importantly, the magnitude of the external field. When the external bias is too strong, disentanglement events are very rare, and all knots will end up being permanently entangled with the gel structure; on the other hand, when it is too weak, the typical disentanglement time is very short, and the dependence of τ_f as a function of the ACN dominates the motion of the polymers, reestablishing the usual linear relationship.

Random Walk Model with Topology-Dependent Rates Captures the Observed Nonmonotonic Behavior

As shown in *DNA Knots Form an Electrophoretic Arc only in Irregular Gels*, 2D electrophoresis experiments and Brownian dynamics simulations of knotted loops in irregular gels are in qualitative agreement in many aspects. In this section, we propose a simple model that reproduces the main findings of the simulations and furnishes a simple but accurate way to predict the arc shapes of the experimental patterns as a function both of the knot complexity and of the loop contour length.

In this model, we describe the knotted loop moving within the irregular gel as a biased random walk on a 1D lattice, i.e., a random walk that moves to the right (direction of the external field) unless it is trapped into an entangled state (due to impalement), with probability $\lambda_e(\mathcal{K}) = \tau_f^{-1}(\mathcal{K})$ (see *Supporting Information* for more details). Once in the entangled state, the walker has to wait a given amount of time that is picked randomly from a bimodal distribution consisting of an exponential decay, modeling the short time disentanglement, and a smaller probability peak at large times, describing the long disentanglement time from a head-on collision (see *Supporting Information* for the details). In this simple description, the only relevant parameters are the hitting rate and the parameters characterizing the bimodal distribution of waiting (i.e., disentanglement) times.

Once the values of these parameters are set to reproduce the data reported in Fig. 3 (see also *Supporting Information*), the model can be used to predict the mobility of the electrophoretic arc as a function of ACN. As shown in Fig. 5, this procedure reproduces with remarkably good agreement the simulation data, and, in particular, it captures the physical mechanism leading to the nonmonotonic mobility at moderate field. Note that, as the random walker solely moves to the right, the field strength enters into the model only through the waiting times and the hitting rates.

More importantly, once the parameter values of the biased random walk model are set for a given pore size of the gel, l_1, their values for a different pore size, l_2, can be estimated from general arguments (see *Supporting Information*). We can therefore use this simplified model to predict the moderate field mobility and the shape of the electrophoretic arcs of DNA knots in gels of variable pore size, e.g., tuned via agarose concentration (36) or nanowire growth cycle (37).

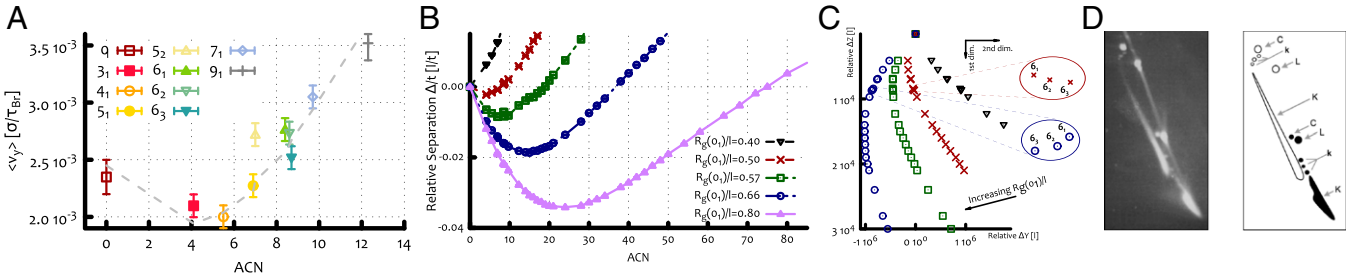

Fig. 5. (*A*) Average speed along the direction of the moderate field from Fig. 2*B*. The dashed line is obtained from the biased continuous random walk model, and corresponds to the (shifted and rescaled) red curve in *B*. (*B*) Average relative separation (in units of lattice spacing over time) of the knots as a function of the ACN for different parameters, as predicted by the continuous random walk model. The gray dashed line in *A* is obtained by shifting the red curve in *B* by the value of $\langle v_y \rangle(0_1)$ and rescaling it by the free velocity v_{free}. (*C*) Reconstruction of a 2D gel electrophoresis experiment from the data in *B* and zoom over the relative position of the family of six-crossings knots for two cases in which the minimum of the arc is at their left and their right. (*D*) Outcomes of a 2D gel electrophoresis experiments performed on P4 viral DNA with different lengths, respectively 4.7 (black) and 10 (white) kbp at equal agarose concentration (0.4%) [reprinted with permission from ref. 29 (Trigueros and Roca)].

The plots presented in Fig. 5*B* and Fig. S4 suggest that tighter gels give rise to more curved (or deeper) arcs where the slowest knot has a higher ACN with respect to sparser gels. Moreover, because the entanglement rate λ_e and the disentanglement time $\tau_{\rm dis}$ (both of these relative to the same quantities for the unknot) should depend only on the ratio between the knot extension and the gel pore size l, a similar trend should also be observed by increasing the DNA loop contour length by keeping fixed l (see *Supporting Information*). This is in qualitative agreement with experiments, as electrophoretic arcs are straighter for shorter DNA molecules (Fig. 5*D*). A further quantitative prediction we can draw from our arguments is that the relative position of the three six-crossing knots can be controlled by tuning the pore size (Fig. 5) of the gel. Indeed, the size of the pores determines whether the 6_1 Stevedore's knot is to the left or to the right of the minimum of the mobility curve: In the former case, 6_1 will moves faster in the gel than the 6_2 and 6_3 knots (which, having higher can, also have higher AEN), whereas, in the latter case, it will move more slowly. This detailed prediction could be tested in future electrophoresis experiments with knotted DNA loops moving within different gels.

Conclusions

We have studied the role of topology in the gel electrophoretic mobility of DNA knots by means of Brownian dynamics simulations and a minimal model of biased random walk. We showed that, when the knots are driven through a physical gel, i.e., one possessing dangling ends, the knots' mobility, as a function of their ACN, depends on the strength of the external field.

At weak fields, we recover the well-known linear relationship between migrating speed and knot type; at stronger fields, we observe instead a nonmonotonic behavior. We argue that this puzzling feature, routinely observed in experiments but not yet fully explained, can be better understood by taking into account the topological interactions, or entanglements, of the knots with the irregularities of the surrounding gel. Although more-complex knots assume more-compact configurations, and hence smaller Stokes friction than simpler knots, they also experience more-complex entanglements with the gel and, hence, longer disentanglement times. These two competing effects give rise to the nonmonotonic speed of the knots observed in the experiments, a feature that, remarkably, is absent for knotted loops moving in a regular gel (i.e., no dangling ends). Although most of our simulations were performed with a rigid gel, we tested that the results are qualitatively unchanged for gels with flexible dangling ends (see *Materials and Methods* and *Supporting Information* and Fig. S5).

We also propose a model that describes the motion of knotted DNA loops as a biased continuous-time random walk. This model, although minimal, by focusing on the competition between Stokes friction and topological entanglements highlighted by the simulations, is able to predict the shape of electrophoretic patterns of DNA knots of different contour length observed in gels with tunable physical properties. In particular, we predict that, by changing the ratio between the radius of gyration of the unknot and the gel pore size, 2D gel electrophoresis experiments should lead to deep electrophoretic arcs for tight gels (or long knots), and shallow ones for sparse gels (or short knots).

We hope that our results will prompt further experimental and numerical verification of the role of topology in the anomalous electrophoretic mobility of knotted polymers and, consequently, suggest new and more accurate setups to separate biopolymers of different topology. Lastly, we highlight that it may be possible to understand the patterns of DNA molecules with different densities of supercoiling within the presented framework as a similar competition between loop size and loop–gel interactions may be responsible for their characteristic behavior.

Materials and Methods

Double-stranded (ds) and nicked, i.e., torsionally relaxed, DNA (dsDNA) knots are modeled as closed and knotted semiflexible bead-spring chains (38), with beads of diameter $\sigma = 2.5$ nm, which reflects the thickness of hydrated B-DNA near physiological conditions (39). The persistence length is set to $l_p = 20\sigma = 50$ nm, and the chosen contour length $L_c = 512\sigma$ corresponds to DNA loops of length ~ 4 kbp $\simeq 1.3$ μm.

The gel is modeled as an imperfect and rigid cubic mesh, with lattice spacing $l = 80\sigma \simeq 200$ nm compatible with the average pore size of agarose gels at 5% and artificial gels made of solid nanowires (36, 37) (for more details on the model and comparison with the case of flexible dangling ends, see *Supporting Information*). The irregularities, or dangling ends, of the gel are created by starting from a regular cubic mesh and then halving some of the edges randomly, with probability $p = 0.4$. Although this probability is chosen arbitrarily, it is possible to map it to a real value of disorder found in an agarose gel at a given concentration by comparing the mobility of linear and ring polymers running through it, similarly to what was done in ref. 20. The edges of the mesh are discretized with beads of size $\sigma_g = 10\sigma \simeq 25$ nm, which is compatible with the observed diameter of agarose bundles (36, 40, 41). For simplicity and computational efficiency, we model the gel as a static mesh, meaning that the mesh structure is not deforming under either thermal of mechanical strains. This is an approximation for an agarose gel, whose bundles are generally, at the concentrations used in gel electrophoresis, found to be made of tens of fibers whose persistence length has been observed to be around 2 – 10 nm (40). In light of this, a conservative estimation of the persistence length of an agarose bundle is comparable with that of DNA, i.e., $l_p \simeq 50$ nm (this assumes weak attraction between the fibers; see *Supporting Information*). In this case, whose analysis is detailed in *Supporting Information*, we do not observe significant deviations from the results presented here in *DNA Knots Form an Electrophoretic Arc only in Irregular Gels*. It is also worth noticing that this perfectly rigid environment closely resembles artificial gels made of solid nanowires (37), which possess a much higher Young modulus and have been found to be optimal media for gel electrophoresis experiments.

The external field is modeled as a force $\boldsymbol{f}$ acting on each bead forming the polymers. Assuming that, in physiological conditions, half of the charges from the phosphate groups are screened by counter ions (42), one can think that each bead ($\sigma = 2.5$ nm $\simeq 8$ bp) contains a total charge of $q_b = 16 q_e/2$, where q_e is the electron charge. Within this assumption, we can map the external force applied onto each bead to an effective electric field $\boldsymbol{E} = \boldsymbol{f}/q_b$. Although this mapping is a crude approximation of the Coulomb interaction between the charged DNA, the ions in solution, and the applied electric field, we find that we can recover a weak field behavior of the knotted samples, i.e., linear increase of the speed as a function of their ACN, up to ~ 50 V/cm, which is roughly comparable with the field intensity used in experiments. In this work, we used field intensities in the range from $E = 1.25$ V/cm to $E = 625$ V/cm.

The ACNs used in this work were obtained from ref. 43, where the authors computed the ACN corresponding to Möbius energy minimizing knotted configurations. The thermally averaged ACN of the samples used in this work has been computed from equilibrated configurations and has been found to be in a one-to-one correspondence to the values in ref. 43, confirming the linear relationship between the ACN of ideal and thermally agitated configurations (17).

The hydrodynamics is here considered only implicitly, as is customary for Brownian dynamics simulations. This means that the polymers do not feel one another via hydrodynamical interactions but are subject to thermal fluctuations due to a surrounding bath at fixed temperature T (see *Supporting Information* for more details).

The simulation time scale is given in terms of the Brownian time, which corresponds to the time taken by a bead of size σ to diffuse its own size, i.e., $\tau_{Br} = \sigma^2/D_\sigma$, where $D_\sigma = k_B T/\xi = k_B T(3\pi\eta_{sol}\sigma)^{-1}$ is the diffusion coefficient of one bead and $\eta_{sol} = 10$ cP (centipoise) is the solution (water) viscosity. From this, we obtain $\tau_{Br} = 3\pi\eta_{sol}\sigma^3/k_B T \simeq 40$ ns.

ACKNOWLEDGMENTS. D. Michieletto acknowledges support from the Complexity Science Doctoral Training Centre at the University of Warwick with funding provided by the Engineering and Physical Sciences Research Council (EPSRC) (EP/E501311). The computing facilities were provided by the Centre for Scientific Computing of the University of Warwick with support from the Science Research Investment Fund. D. Marenduzzo thanks EPSRC Grant EP/I034661/1 for support. E.O. acknowledges support from the Italian Ministry of Education Grant PRIN 2010HXAW77.

1. Calladine CR, Drew H, Luisi FB, Travers AA (1997) *Understanding DNA: The Molecule and How It Works* (Elsevier, New York).
2. Bates A, Maxwell A (2005) *DNA Topology* (Oxford Univ Press, New York).
3. Olavarrieta L, et al. (2002) Supercoiling, knotting and replication fork reversal in partially replicated plasmids. *Nucleic Acids Res* 30(3):656–666.
4. Cebrián J, et al. (2014) Electrophoretic mobility of supercoiled, catenated and knotted DNA molecules. *Nucleic Acids Res* 43(4):e24.
5. Stasiak A, Katritch V, Bednar J, Michoud D, Dubochet J (1996) Electrophoretic mobility of DNA knots. *Nature* 384(6605):122.
6. Arsuaga J, et al. (2005) DNA knots reveal a chiral organization of DNA in phage capsids. *Proc Natl Acad Sci USA* 102(26):9165–9169.
7. de Gennes PG (1979) *Scaling Concepts in Polymer Physics* (Cornell Univ Press, Ithaca, NY).
8. Rubinstein M (1987) Discretized model of entangled-polymer dynamics. *Phys Rev Lett* 59(17):1946–1949.
9. Duke TA (1989) Tube model of field-inversion electrophoresis. *Phys Rev Lett* 62(24): 2877–2880.
10. Viovy JL, Duke T (1993) DNA electrophoresis in polymer solutions: Ogston sieving, reptation and constraint release. *Electrophoresis* 14(4):322–329.
11. Barkema GT, Marko JF, Widom B (1994) Electrophoresis of charged polymers: Simulation and scaling in a lattice model of reptation. *Phys Rev E Stat Phys Plasmas Fluids Relat Interdiscip Topics* 49(6):5303–5309.
12. Viovy J (2000) Electrophoresis of DNA and other polyelectrolytes: Physical mechanisms. *Rev Mod Phys* 72(3):813–872.
13. Vologodskii AV, et al. (1998) Sedimentation and electrophoretic migration of DNA knots and catenanes. *J Mol Biol* 278(1):1–3.
14. Weber C, Carlen M, Dietler G, Rawdon EJ, Stasiak A (2013) Sedimentation of macroscopic rigid knots and its relation to gel electrophoretic mobility of DNA knots. *Sci Rep* 3:1091.
15. Piili J, Marenduzzo D, Kaski K, Linna RP (2013) Sedimentation of knotted polymers. *Phys Rev E Stat Nonlin Soft Matter Phys* 87(1):012728.
16. Weber C, Stasiak A, De Los Rios P, Dietler G (2006) Numerical simulation of gel electrophoresis of DNA knots in weak and strong electric fields. *Biophys J* 90(9): 3100–3105.
17. Katritch V, et al. (1996) Geometry and physics of knots. *Nature* 384:142–145.
18. Trigueros S, Arsuaga J, Vazquez ME, Sumners DW, Roca J (2001) Novel display of knotted DNA molecules by two-dimensional gel electrophoresis. *Nucleic Acids Res* 29(13):E67.
19. Arsuaga J, Vázquez M, Trigueros S, Sumners D, Roca J (2002) Knotting probability of DNA molecules confined in restricted volumes: DNA knotting in phage capsids. *Proc Natl Acad Sci USA* 99(8):5373–5377.
20. Michieletto D, Baiesi M, Orlandini E, Turner MS (2015) Rings in random environments: Sensing disorder through topology. *Soft Matter* 11(6):1100–1106.
21. Mickel S, Arena V, Jr, Bauer W (1977) Physical properties and gel electrophoresis behavior of R12-derived plasmid DNAs. *Nucleic Acids Res* 4(5):1465–1482.
22. Levene SD, Zimm BH (1987) Separations of open-circular DNA using pulsed-field electrophoresis. *Proc Natl Acad Sci USA* 84(12):4054–4057.
23. Turmel C, Brassard E, Slater GW, Noolandi J (1990) Molecular detrapping and band narrowing with high frequency modulation of pulsed field electrophoresis. *Nucleic Acids Res* 18(3):569–575.
24. Åkerman B, Cole KD (2002) Electrophoretic capture of circular DNA in gels. *Electrophoresis* 23(16):2549–2561.
25. Cole KD, Åkerman B (2003) The influence of agarose concentration in gels on the electrophoretic trapping of circular DNA. *Sep Sci Technol* 38(10):2121–2136.
26. Robertson RM, Smith DE (2007) Strong effects of molecular topology on diffusion of entangled DNA molecules. *Proc Natl Acad Sci USA* 104(12):4824–4827.
27. Stellwagen NC, Stellwagen E (2009) Effect of the matrix on DNA electrophoretic mobility. *J Chromatogr A* 1216(10):1917–1929.
28. Adams CC (1994) *The Knot Book: An Elementary Introduction to the Mathematical Theory of Knots* (Freeman, New York).
29. Trigueros S, Roca J (2007) Production of highly knotted DNA by means of cosmid circularization inside phage capsids. *BMC Biotechnol* 7:94.
30. Mohan A, Doyle PS (2007) Stochastic modeling and simulation of DNA electrophoretic separation in a microfluidic obstacle array. *Macromolecules* 40(24):8794–8806.
31. Mohan A, Doyle PS (2007) Effect of disorder on DNA electrophoresis in a microfluidic array of obstacles. *Phys Rev E Stat Nonlin Soft Matter Phys* 76(4 Pt 1):040903.
32. Dorfman KD (2010) DNA electrophoresis in microfabricated devices. *Rev Mod Phys* 82(4):2903–2947.
33. Michieletto D, Marenduzzo D, Orlandini E, Alexander G, Turner M (2014) Threading dynamics of ring polymers in a gel. *ACS Macro Lett* 3:255–259.
34. Michieletto D, Marenduzzo D, Orlandini E, Alexander GP, Turner MS (2014) Dynamics of self-threading ring polymers in a gel. *Soft Matter* 10(32):5936–5944.
35. Weber C, De Los Rios P, Dietler G, Stasiak A (2006) Simulations of electrophoretic collisions of DNA knots with gel obstacles. *J Phys Condens Matter* 18(14):S161–S171.
36. Pernodet N, Maaloum M, Tinland B (1997) Pore size of agarose gels by atomic force microscopy. *Electrophoresis* 18(1):55–58.
37. Rahong S, et al. (2014) Ultrafast and wide range analysis of DNA molecules using rigid network structure of solid nanowires. *Sci Rep* 4:5252.
38. Kremer K, Grest GS (1990) Dynamics of entangled linear polymer melts: A molecular-dynamics simulation. *J Chem Phys* 92(8):5057.
39. Rybenkov VV, Cozzarelli NR, Vologodskii AV (1993) Probability of DNA knotting and the effective diameter of the DNA double helix. *Proc Natl Acad Sci USA* 90(11):5307–5311.
40. Guenet JM, Rochas C (2006) Agarose sols and gels revisited. *Macromol Symp* 242(1): 65–70.
41. Sugiyama J, Rochas C, Turquois T, Taravel F, Chanzy H (1994) Direct imaging of polysaccharide aggregates in frozen aqueous dilute systems. *Carbohydr Polym* 23(4): 261–264.
42. Maffeo C, et al. (2010) DNA–DNA interactions in tight supercoils are described by a small effective charge density. *Phys Rev Lett* 105(15):158101.
43. Kusner R, Sullivan J (1994) Möbius energies for knots and links, surfaces and submanifolds. *Geometric Topology: Proceedings of the 1993 Georgia International Topology Conference*, ed Kazez WH (Am Math Soc, Cambridge, MA), pp 570–604.
44. Mogilner A, Rubinstein B (2005) The physics of filopodial protrusion. *Biophys J* 89(2): 782–795.